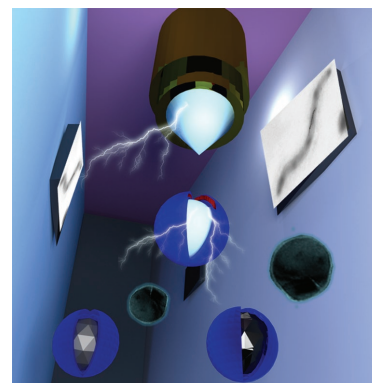


# Manufacturing Man-Made Magnetosomes: High-Throughput In Situ Synthesis of Biomimetic Magnetite Loaded Nanovesicles

Poonam K. Bakhshi, Jennifer Bain, Mine Orlu Gul, Eleanor Stride, Mohan Edirisinghe,\* Sarah S. Staniland\*

A new synthetic method for the production of artificial magnetosomes, i.e., lipid-coated vesicles containing magnetic nanoparticles, is demonstrated. Magnetosomes have considerable potential in biomedical and other nanotechnological applications but current production methods rely upon magnetotactic bacteria which limits the range of sizes and shapes that can be generated as well as the obtainable yield. Here, electrohydrodynamic atomization is utilized to form nanoscale liposomes of tunable size followed by electroporation to transport iron into the nanoliposome core resulting in magnetite crystallization. Using a combination of electron and fluorescence microscopy, dynamic light scattering, Raman spectroscopy, and magnetic susceptibility measurements, it is shown that single crystals of single-phase magnetite can be precipitated within each liposome, forming a near-monodisperse population of magnetic nanoparticles. For the specific conditions used in this study the mean particle size is 58 nm ( $\pm 8$  nm) but the system offers a high degree of flexibility in terms of both the size and composition of the final product.



Dr. P. K. Bakhshi, Prof. M. Edirisinghe  
Department of Mechanical Engineering  
University College London, Roberts  
Torrington Place, London WC1E 7JE, UK  
E-mail: m.edirisinghe@ucl.ac.uk

Dr. J. Bain, Dr. S. S. Staniland  
Department of Chemistry  
University of Sheffield  
Brook Hill, Sheffield S3 7HF, UK  
E-mail: s.s.staniland@sheffield.ac.uk

Dr. M. Orlu Gul  
School of Pharmacy  
Department of Pharmaceutics  
University College London  
29/39 Brunswick Square, London WC1N 1AX, UK  
Prof. E. Stride

Institute of Biomedical Engineering  
University of Oxford  
Old Road Campus, Research Building  
University of Oxford  
Oxford OX3 7DQ, UK

This is an open access article under the terms of the Creative Commons Attribution License, which permits use, distribution and reproduction in any medium, provided the original work is properly cited.

The copyright line was changed 25 October after initial publication.

## 1. Introduction

Magnetic nanoparticles (MNPs) continue to be the subject of extensive research owing to their potential to offer transformative improvements in a wide range of applications including magnetic separation,<sup>[1]</sup> ultrahigh density data storage,<sup>[2]</sup> catalysis,<sup>[3]</sup> and increasingly the important field of nanomedicine. Magnetite nanoparticles ( $\text{Fe}_3\text{O}_4$ ) in particular are used in numerous advanced diagnostic and therapeutic applications including magnetic resonance imaging (MRI) contrast agents and targeted magnetic hyperthermia treatment of tumours.<sup>[4–8]</sup> Magnetite is stable, non-toxic, and has the highest magnetic saturation of all the iron oxides with  $\text{Fe}^{2+}$  and  $\text{Fe}^{3+}$  centres in a 1:2 ratio ( $\text{Fe}^{2+}\text{Fe}^{3+}_2\text{O}_4$ ).<sup>[9]</sup> Spherical magnetite nanoparticles are superparamagnetic below  $\approx 30$  nm and exhibit multi-domain magnetic characteristics above  $\approx 90$  nm at ambient temperature. Between this range the MNPs are single-domain ferrimagnets offering the highest magnetic saturation per volume, making them optimal for many medical and nanotechnological applications. Magnetite can be formed simply by raising the pH of a mixed valence iron solution under an inert atmosphere to precipitate the oxide. However, this often leads to a

heterogeneous population of particle size, shape, and contamination with other iron oxides. More uniform populations of pure magnetite nanoparticles can be produced, but only via multistep processes involving increased temperature, pressure, and/or toxic reagents.<sup>[10]</sup> It remains a significant challenge to produce aqueous suspensions of monodisperse, single-domain magnetite nanoparticles under ambient conditions.

Magnetotactic bacteria (MTB) are heterogeneously diverse aquatic microbes that possess the ability to align and swim along magnetic field lines. Under microaerobic conditions they take up iron ions from the environment and produce intracellular nanoparticles of magnetite. The nanoparticles, which are “single-domain” magnets and underlay the cells’ magnetotaxis, form within lipid vesicles termed “magnetosomes.”<sup>[11,12]</sup> The MNP size ranges from 40 to 100 nm in diameter depending on the species and since their discovery MTB have provided the inspiration to develop biomineralization routes to obtain homogeneous single-domain MNPs.<sup>[13]</sup> To form the MNP, the internal liposome is first invaginated from the bacteria’s cytoplasmic membrane and in doing so recruits a series of biomineralization proteins<sup>[14]</sup> that orchestrate the process of MNP crystallization by: (i) importing iron ions into the liposome, (ii) maintaining the correct chemical environment within the liposome for magnetite to form (i.e., correct redox potential, high pH), (iii) nucleating the iron ions to initiate crystallization, and (iv) controlling crystallization precisely to produce an MNP of a fixed size and morphology.<sup>[15–17]</sup>

The merits of using magnetosomes for biomedical applications are well established. The phospholipid bilayer surrounding the magnetosome is readily functionalizable with various biological moieties for their use in biomedical applications and extensive research has been carried out to exploit this.<sup>[18]</sup> Native bacterial proteins have been thoroughly investigated as anchor sites for the expression of foreign proteins (e.g., Protein A, luciferase, and acetate kinase) on the surface of the magnetosome.<sup>[19]</sup> In magnetic hyperthermia, magnetosomes<sup>[20]</sup> and magnetically modified magnetosomes<sup>[21]</sup> have been shown to be superior to equivalent synthetically produced MNPs.<sup>[22]</sup> However, magnetosomes have several disadvantages: the extent to which magnetosomes can be modified within the bacteria is very restricted due to cell toxicity, furthermore the MTB are slow-growing and difficult to cultivate. The large-scale fermenter growth of several magnetic bacteria has also been performed and this has seen improved yields leading to the hope of realizing technological exploitation. However, biomineralization in magnetic bacteria, even in an improved fermenter system, is a highly inefficient method of producing MNPs, with low yields presenting a barrier to the successful commercialization of the magnetosomes. The utilization of magnetosomes for more varied MNP applications has also been limited due to the fact that the magnetic properties of magnetosomes cannot be varied due to the bacteria’s specificity for iron.<sup>[23]</sup> Attempts have been made to address these issues by developing biomimetic approaches to produce artificial magnetosomes that can be more readily scaled up and adapted to achieve

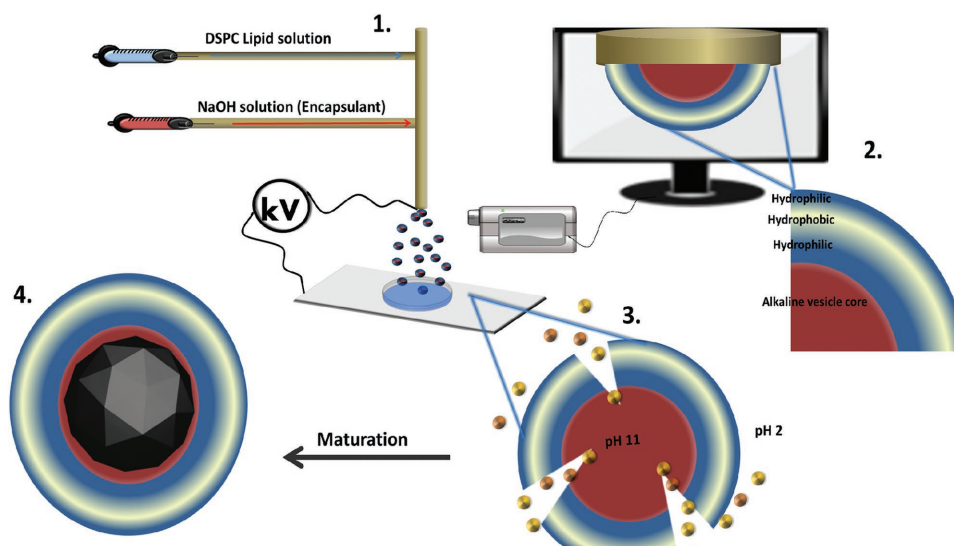


**Figure 1.** Methodology of the synthesis. Schematic diagram showing experimental setup for the electrohydrodynamic production of artificial magnetosomes: (1) encapsulation of NaOH within DSPC liposomes via the EHDA jetting system, (2) showing the composition of the EHDA formed vesicles, (3) before being introduced to mixed valence iron solution and consequently electroporated at 750 V, and (4) to yield a magnetic nanoparticle within the vesicle core (artificial magnetosome).

particular particle characteristics but currently these are subject to the same challenges as conventional inorganic protocols.<sup>[24–26]</sup> Our aim in this study was to develop a synthetic process that mimics magnetosome formation (Figure 1) and hence enables control over MNP formation, size, and lipid coating, while also offering much greater flexibility to adapt the system and increase yield.

## 2. Results

The process involves two steps: first, controlled high-throughput production of liposomes was achieved using electrohydrodynamic atomization (EHDA), which offers a scalable means of generating tunable uniformed nanosized vesicles.<sup>[27,28]</sup> EHDA utilizes a high electrical potential difference to induce focusing and break up of a liquid jet into small droplets.<sup>[27–29]</sup> In this study, a syringe pump was used to generate a steady flow of lipid/base suspension through a stainless steel bi-port needle at  $20 \mu\text{L min}^{-1}$  and an electrical potential difference of 16.8–17.5 kV was applied to generate continuous stable jetting (see Sections S1 and S2, Supporting Information).

1,2-Distearoyl-*sn*-glycero-3-phosphocholine lipid (DSPC) was used which self-assembles into a high volume (73% yield, Section S3, Supporting Information) of near-monodisperse nanoliposomes when accelerated by jetting through the EHDA needle outlet; mimicking the invagination of the cytoplasmic membrane to form the empty magnetosome. The size of the resulting liposomes was found to be  $\approx 22 \text{ nm} \pm 4.8 \text{ nm}$  by dynamic light scattering (DLS) analysis and these results were supported by measurements from transmission electron microscopy (TEM) images (Figure 2).

DSPC can be difficult to work with in more traditional liposome synthesis methods, such as sonication or extrusion<sup>[30]</sup> owing to its high glass transition temperature ( $T_g$ ). For DSPC the lipid solution must be kept above  $55 \text{ }^\circ\text{C}$  for it to remain amorphous, as below this critical temperature the lipid will be in the gel phase and can easily precipitate out of solution. This was evident during control tests of synthesis by tip sonication (Figure S4, Supporting Information). TEM analysis of liposomes prepared by both methods shows distinct differences. Those prepared by EHDA show clear vesicles with a near monodisperse distribution (Figure 2), which is in stark contrast to the sonicated control sample in which vesicles appeared to have been severely damaged by the preparation method (Figure S4a, Supporting Information). This can be attributed to the  $T_g$  of DSPC and different working temperatures of each method. It is possible that the negative effects of  $T_g$  are not observed in the EHDA prepared sample due to the application of the high voltage

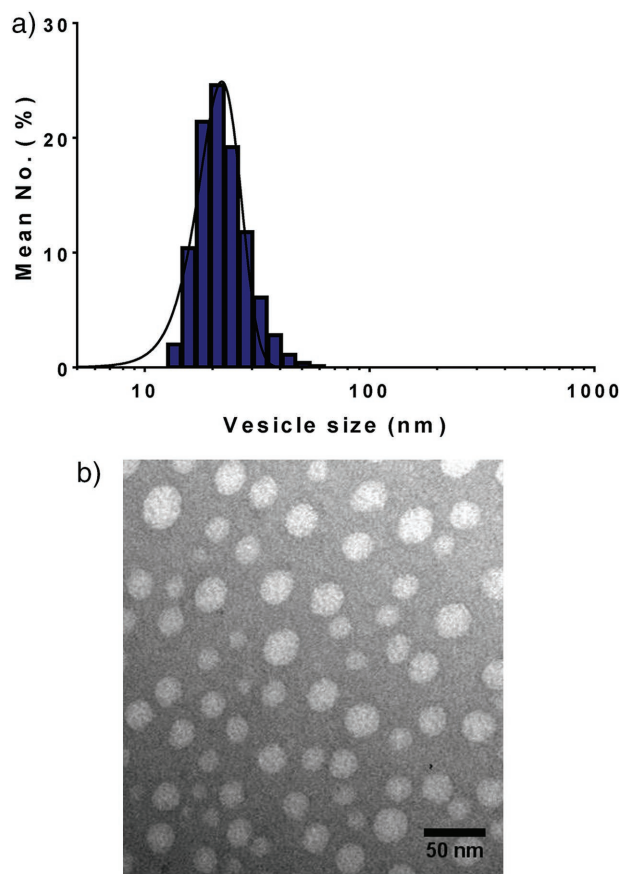


**Figure 2.** Size distribution of vesicles. a) The size distribution of non-electroporated liposomes obtained by DLS. b) TEM images of the NaOH encapsulated vesicles formed at optimized conditions (200  $\mu\text{m}$  diameter, 96 mm needle length,  $20 \mu\text{L min}^{-1}$  flow rate, 16.8–17.5 kV voltage).

during the continuous flow and rapid formation process, ensuring that the DSPC remains in the amorphous phase throughout. The application of the high voltage is not only responsible for the rapid formation of nanovesicles but also appeared to assist in the formation of a vesicular structure, hugely increasing their stability, compared with liposomes formed by tip sonication. EHDA formed liposomes remained stable for the studied period of 120 d (Figure 2).

Liposomes were then used as nanoreactors for magnetite mineralization. Magnetite is only able to precipitate within vesicles if iron ions ( $\text{Fe}^{2+}$ ,  $\text{Fe}^{3+}$ ) in solution surrounding the vesicle are transported into the interior to achieve an optimum concentration to induce nucleation.<sup>[31]</sup> Electroporation is widely used in molecular biology for the introduction of DNA or nucleic acids into cells.<sup>[32]</sup> The authors recently demonstrated that electroporation can also be utilized to open pores in the membrane for the in situ precipitation of MNPs

in polymersome membranes,<sup>[33]</sup> and a similar approach was adopted in this study to permeabilize the DSPC liposomes. Application of a localized high electric field induces the reversible poration of the lipid membrane, enabling the transportation of iron ions across the membrane into the liposome core, mimicking the role of the transmembrane ion-transport proteins found in the MTB magnetosome.

The electroporation conditions were optimized (voltage = 750 V, pulse duration = 100  $\mu$ s, and number of pulses = 9) for the EHDA synthesized liposomes to maximize iron ions transport across the membrane. The pH gradient established across the membrane initiates the transport of iron ions ( $\text{Fe}^{2+}$ ,  $\text{Fe}^{3+}$ ) through the pores opened by electroporation.<sup>[34]</sup> Inside the liposomes, the iron ions react with NaOH (0.1 M) to form magnetite.<sup>[35,36]</sup> Figure 3 shows that electroporation of EHDA synthesized DSPC liposomes results in the crystallization of a single magnetite nanoparticle within the liposome core, forming a near monodisperse population of artificial magnetosome 58 nm  $\pm$  8 nm (Figure 3). It is of note that

these artificial magnetosomes are of comparable size and structure to natural magnetosomes, with the uniformed MNP filling the vesicle core. The mean size of the magnetosomes is increased compared to that of the precursor vesicles (22 nm), which may be due to agglomeration of vesicles during electroporation. Given that the EHDA method enables the initial vesicle size to be very tightly controlled by varying the processing parameters, it offers excellent opportunities for tuning magnetosome size to suit a given application.

Raman spectroscopy was used to confirm both the material composition of the magnetite nanoparticle formation and the presence of the lipid bilayer observed in TEM (Figure 4). Significant peaks were observed at 662, 533–553, and 230  $\text{cm}^{-1}$  indicating magnetite.<sup>[37]</sup> The peaks seen at 750 and 1100  $\text{cm}^{-1}$  correspond to the presence of a phosphatidylcholine bilayer. However, Raman spectroscopy provides no spatial information, so fluorescence assays were employed to determine if the MNP is surrounded with lipid as suggested by TEM analysis (Figure 4b). Using the lipophilic dye BODIPY FL  $\text{C}_5$ -ceramide (*N*-(4,4-difluoro-5,7-dimethyl-4-bora-3a,4a-diaza-*s*-indacene-3-pentanoyl)spingosine, Life Technologies) discrete fluorescent vesicles were observed only in the magnetically separated and washed artificial magnetosome sample. Furthermore when placed in a magnetic field, movement of the discrete fluorescent vesicles was observed (Figure S5, Supporting Information). This was not the case for suspensions of uncoated MNP or pre-electroporated liposomes used as a control.

To confirm the presence of magnetic material, magnetic hysteresis and field-cooled/zero-field-cooled magnetic susceptibility measurements as a function of temperature were performed (Figure 5). The data clearly show the presence of magnetic material and a magnetic structural phase transition at 118 K, known as the Verwey transition (Figure 5).<sup>[38]</sup> In magnetite the cubic magnetocrystalline axis switches from the body diagonal to the cube edge resulting in a magnitude loss of magnetic remnants through the Verwey transition, providing a simple magnetic fingerprint for magnetite. This indicates that single-domain magnetite crystals were indeed crystallized within the EHDA synthesized nanoliposomes.

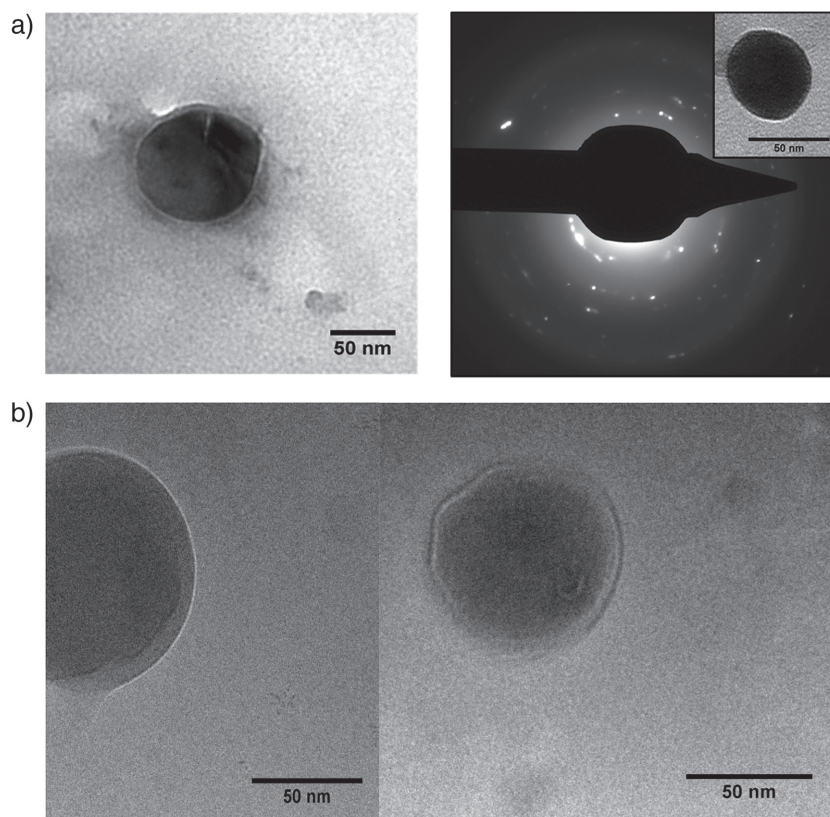


**Figure 3.** The effect of electroporation on nanovesicles. Unstained nanoliposomes subjected to optimized (100  $\mu$ s pulse duration, 9 pulses, 750 V) electroporation conditions show MNP crystallized in their interior. a) Left: Ambient temperature (298 K); right: selected area electron diffraction pattern of artificial magnetosome at room temperature (inset: corresponding artificial magnetosome TEM image). b) Cryogenic (77 K) TEM images.

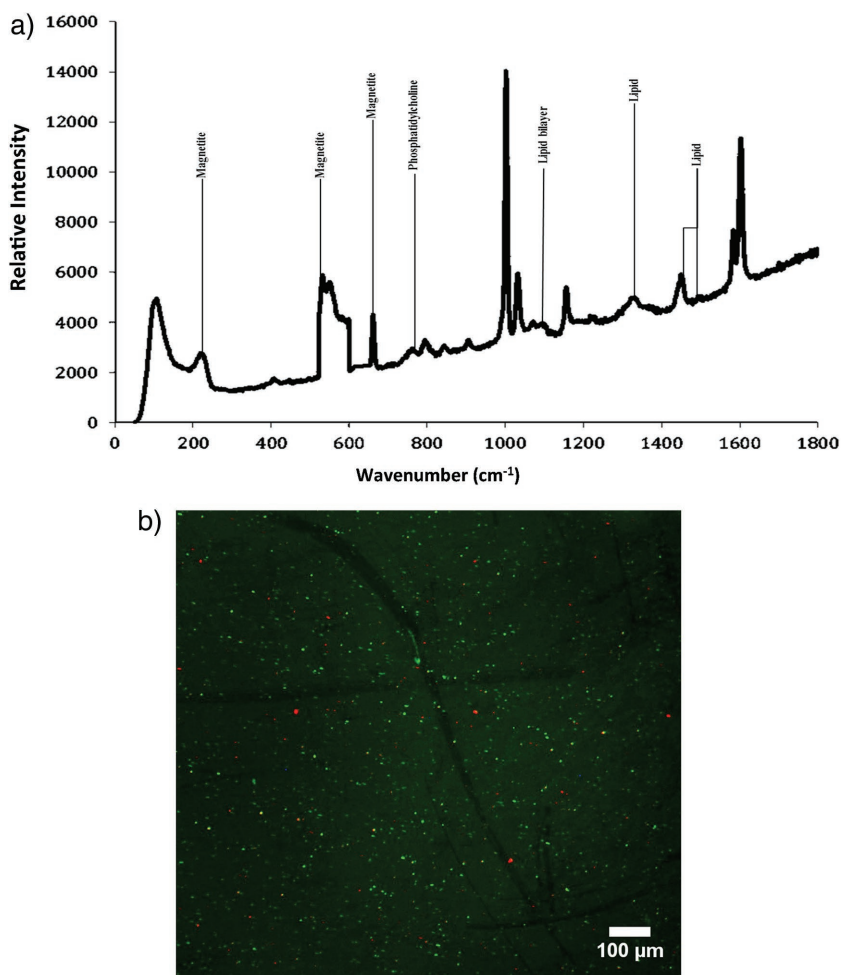


**Figure 4.** The characterization of the iron oxide within the nanovesicles. a) Raman spectrum of artificial magnetosomes shows DSPC lipid encapsulating magnetite. Spectrum shows the presence of peaks representative of magnetite (at 230, 535, and 665  $\text{cm}^{-1}$ ) and a phosphatidylcholine lipid bilayer (peaks highlighted at  $\text{cm}^{-1}$  and above). b) Lipophilic fluorescent dye incorporation (Bodipy), showing the presence of magnetically responsive (Figure S5, Supporting Information) liposomes.

reported (Figure S6, Supporting Information) using a different lipid (DOPC) to form magnetoliposomes. The aim of this study was to demonstrate the feasibility of the method for forming magnetosomes, but we have also shown in previous work that particle size can be readily tuned by varying the combination of flow rate, electrical potential difference, and liquid properties (density, viscosity, and surface tension) used in EHDA processing.<sup>[27,28]</sup>

As highlighted in the Introduction, magnetosomes are very attractive nanomagnetic materials for nanotechnological applications due to their excellent size and shape definition. Potential applications range from information storage, e.g., high-density multi-dimensional recording, high-frequency electronics and spintronics, to targeted medical diagnostics and therapies, e.g., contrast agents for MRI imaging, site-specific chemotherapy, and hyperthermic cancer treatments. They are inherently biocompatible, stable, and easily dispersed due to their intrinsic lipid coating which, as above, can also be readily functionalized, e.g., by inclusion of functional proteins to which antibodies can be conjugated. Once again the flexibility of EHDA in this respect is a considerable advantage as different types of coating material can be readily substituted to facilitate the required surface functionalization.

In this study a flow rate of 20  $\mu\text{L min}^{-1}$  was used for generating the liposomes, yielding 440 mg of NaOH filled DSPC vesicles per 0.6 mL in 30 min. Assuming maximum conversion to magnetoliposomes on electroporation this equates to a theoretical artificial magnetosome yield of 3.7  $\text{kg L}^{-1} \text{d}^{-1}$  (Section S3, Supporting Information) which represents a significant increase on the yields currently achievable for natural magnetosomes from MTB of 0.168  $\text{g L}^{-1} \text{d}^{-1}$ .<sup>[39]</sup> Furthermore, the technology already exists to engineer a scaled-up system with multiple processing channels in parallel with increased flow rates for higher volume throughput to realize orders of magnitude greater yields in shorter harvesting times.<sup>[40]</sup> The flexibility of the EDHA system for producing a range of artificial magnetosomes can also be readily demonstrated. For example, a proof-of-concept study is

### 3. Conclusions

In conclusion, a simple high-throughput method has been demonstrated for producing single-domain magnetite nanoparticles in situ within liposomes, mimicking the production of magnetosomes within MTB. This has a number of important advantages. First, it provides a simplified abiotic model of the biomineralization process. This model system could be used to probe the biomineralization process itself by sequentially inserting biomineralization proteins to better understand their function. Second and crucially, the system enables the development of a scalable route for creating monodisperse populations of lipid-encapsulated single-domain MNPs. The system is highly versatile, offering the potential to produce artificial magnetosomes with

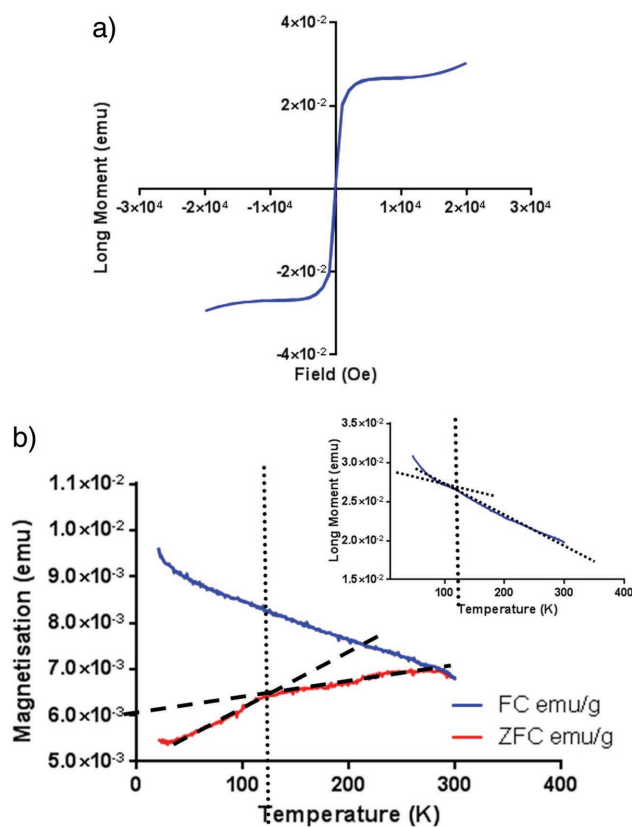


**Figure 5.** Magnetic properties of the artificial magnetosomes. Magnetization measurements at 300 K. a) Magnetization versus field hysteresis plot shows the soft magnetic material characteristic of magnetite. b) ZFC and FC magnetisation versus temperature plot at 100 Oe. Inset shows remnance. The Verwey transition has been shown by — and the temperature at which it occurs has been highlighted (118 K).

a range of properties and sizes that cannot be achieved with natural magnetosomes.

## 4. Experimental Section

**Materials:** All reagents were purchased from Sigma Aldrich. DSPC was dissolved in ethanol ( $10 \times 10^{-3}$  M). 0.1 M solutions of NaOH,  $\text{FeCl}_2 \cdot 4\text{H}_2\text{O}$ , and  $\text{FeCl}_3 \cdot 6\text{H}_2\text{O}$  were prepared in milli-Q  $\text{H}_2\text{O}$  degassed with  $\text{N}_2$  to prevent oxidation.  $\text{Fe}^{3+}$  and  $\text{Fe}^{2+}$  iron solution were used in ratio of 2:1, respectively.

**EHDA Synthesis of Liposomes:** Liposomes were prepared by means of a single bi-port needle (200  $\mu\text{m}$  internal diameter and 96 mm length). This was connected via silicone tubing to syringes containing DSPC ( $10 \times 10^{-3}$  M) solution and sodium hydroxide (0.1 M) solution mounted on syringe pumps drivers (Harvard Apparatus Ltd.). Solutions were pumped through the needle, which was connected to a high-voltage power supply at 0–30 kV (Glassman High Voltage, Tadley, UK), at a rate of 5–50  $\mu\text{L min}^{-1}$ . Liposome solution was collected in a petri dish 100–120 mm below the needle and loaded on a metallic jack attached to a negative electrode, containing degassed  $\text{H}_2\text{O}$ . The applied voltages

and flow rates were optimized to obtain steady multi-jetting and uniform liposomes (Sections S1 and S2, Supporting Information).

**Control Liposome Analysis:** Vesicle size and distribution were determined by DLS (ZetasizerNano ZS, Malvern Instruments, UK) and TEM (Philips CM 12 (80 kV) stained with 1% uranyl acetate for 10 s). Nanovesicles were analyzed by TEM at regular intervals over 0–120 d to assess stability.

**Electroporation of Liposomes:** Electroporation (ECM 2001 Electro Cell Manipulator, Harvard Apparatus, USA) was performed on pre-formed liposomes (0.5 mL) and iron oxide ( $\text{Fe}^{3+}:\text{Fe}^{2+}$  2:1) solution (0.5 mL) in an electroporation cuvette (BTX, electrode distance 2 mm). Parameters including pulse duration (0–100  $\mu\text{s}$ ), voltage (100–1500 V), and number of pulses (1–9) were optimized for iron oxide precipitation at 100  $\mu\text{s}$ , 750 V, and 9 pulses.

**Electron Microscopy Imaging:** The electroporated samples (5  $\mu\text{L}$ ) were prepared at ambient temperature (25  $^\circ\text{C}$ ) without staining on 400 mesh copper-coated carbon grids (Agar Scientific) before analysis by TEM (FEI Tecnai G2 Spirit) to determine the incorporation of iron into the liposomes. Selected area electron diffraction (SAED) images were collected from a specific artificial magnetosome using the microscope in diffraction mode. Images were collected at  $120 \times 10^{-3}$  m. Cryogenic-EM was used to further investigate the structure of the artificial magnetosomes. 2  $\mu\text{L}$  of sample was added to a carbon film 300 mesh grids (Agar Scientific) and blotted for 6 s (at 100% humidity) and then plunged into liquid ethane using a Vitrobot Mark IV. Samples were visualized on an FEI Tecnai F20 microscope fitted with a Gatan  $4\text{K} \times 4\text{K}$  CCD camera.

**Liposome Bilayer Detection:** Presence of a lipid bilayer was confirmed using lipophilic dye BODIPY FL C5-ceramide (*N*-(4,4-difluoro-5,7-dimethyl-4-bora-3a,4a-diaza-s-indacene-3-pentanoyl) sphingosine) added to an artificial magnetosome suspension (50  $\mu\text{L}$ ) in a 1% v/v ratio and stirred for 12 h to ensure bilayer incorporation. This was compared to a control sample of uncoated magnetic nanoparticles to which Bodipy was added in the same ratio. Both samples were analyzed by fluorescence microscopy (Leica DMI4000) to determine dye uptake.

**Magnetic Analysis:** To determine magnetic properties, samples were prepared by centrifugation (8000 rpm for 10 min). The supernatant was discarded and the sample was washed three times (10 mL of double distilled water bubbled with nitrogen gas). Vesicles were dried on a petri dish at the ambient temperature. Magnetization data were obtained via cryogenic vibrating sample magnetometer or a super quantum conducting interference device magnetometer at different temperatures (ambient to 300  $^\circ\text{C}$ ) and in sweeping fields up to 2.5 T, respectively. Raman spectra were obtained with a confocal Raman spectrometer (Jobin Yvon LABRAM) equipped with an Nd-YAG laser (100 mW, 532.2 nm) and diffraction gratings of 1800 grooves  $\text{mm}^{-1}$ . Detection was performed using a Peltier-cooled, slow-scan, CCD matrix detector.

## Supporting Information

Supporting Information is available from the Wiley Online Library or from the author.

Acknowledgements: P.K.B. and J.B. are joint first authors and contributed equally to this work. This work was supported by the EPSRC (Grant Nos. EP/I032355/2 and EP/I032428/1). For technical support with TEM the authors would like to thank Dr. Svetomir Tzokov (Department of Molecular Biology and Biotechnology, University of Sheffield), Mrs. Nicola Mordan (UCL, Eastman Dental Institute), as well as Dr. Stephen Muench (School of Biomedical Science, University of Leeds) for support with cryogenic TEM. The authors thank Dr. Andrea Rawlings (Department of Chemistry, University of Sheffield) and Dr. Jonathan Bramble (IBIOS, University of Nottingham) for useful discussion and advice on the EFG data. The academic title of the author Jenny Bain, Mohan Edirisinghe as an addition corresponding author, and the acknowledgements section regarding first author ship was updated on November 09, 2016. The copyright line for this article was changed on November 09, 2016 after original online publication.

Received: May 11, 2016; Revised: June 11, 2016;  
Published online: August 4, 2016; DOI: 10.1002/mabi.201600181

Keywords: biomimetic; electrohydrodynamic; magnetosomes; magnetotactic bacteria; nanoparticles

- [1] Q. A. Pankhurst, J. Connolly, S. Jones, J. Dobson, *J. Phys. D: Appl. Phys.* **2003**, *36*, R167.
- [2] J.-M. Hu, Z. Li, L.-Q. Chen, C.-W. Nan, *Nat. Commun.* **2011**, *2*, 553.
- [3] V. Polshettiwar, R. Luque, A. Fihri, H. Zhu, M. Bouhrara, J.-M. Basset, *Chem. Rev.* **2011**, *111*, 3036.
- [4] Q. Pankhurst, N. Thanh, S. Jones, J. Dobson, *J. Phys. D: Appl. Phys.* **2009**, *42*, 224001.
- [5] Q. A. Pankhurst, J. Connolly, S. K. Jones, J. Dobson, *J. Phys. D: Appl. Phys.* **2003**, *36*, R167.
- [6] J.-H. Lee, J.-T. Jang, J.-S. Choi, S. H. Moon, S.-H. Noh, J.-W. Kim, J.-G. Kim, I.-S. Kim, K. I. Park, J. Cheon, *Nat. Nanotechnol.* **2011**, *6*, 418.
- [7] J. Ge, Y. Yin, *Angew. Chem., Int. Ed.* **2011**, *50*, 1492.
- [8] C. H. Ho, C. P. Tsai, C. C. Chung, C. Y. Tsai, F. R. Chen, H. J. Lin, C. H. Lai, *Chem. Mater.* **2011**, *23*, 1753.
- [9] L. Chang, B. D. Rainford, J. R. Stewart, C. Ritter, A. P. Roberts, Y. Tang, Q. Chen, *J. Geophys. Res.: Solid Earth* **2009**, *114*, B07101.
- [10] A. E. Regazzoni, G. A. Urrutia, M. A. Blesa, A. J. G. Maroto, *J. Inorg. Nucl. Chem.* **1981**, *43*, 1489.
- [11] C. Jogler, D. Schüler, *Annu. Rev. Microbiol.* **2009**, *63*, 501.
- [12] R. Blakemore, *Science* **1975**, *190*, 377.
- [13] D. A. Bazylinski, S. Schubbe, *Adv. Appl. Microbiol.* **2007**, *62*, 21.
- [14] M. Tanaka, E. Mazuyama, A. Arakaki, T. Matsunaga, *J. Biol. Chem.* **2011**, *286*, 6386.
- [15] M. Tanaka, Y. Okamura, A. Arakaki, T. Tanaka, H. Takeyama, T. Matsunaga, *Proteomics* **2006**, *6*, 5234.
- [16] D. Schüler, R. B. Frankel, *Appl. Microbiol. Biotechnol.* **1999**, *52*, 464.
- [17] C. Jimenez-Lopez, C. S. Romanek, D. A. Bazylinski, *J. Geophys. Res.: Biogeosci.* **2010**, *115*, G00G03.
- [18] T. Matsunaga, S. Kamiya, *Appl. Microbiol. Biotechnol.* **1987**, *26*, 328.
- [19] T. Matsunaga, T. Suzuki, M. Tanaka, A. Arakaki, *Trends Biotechnol.* **2007**, *25*, 182.
- [20] M. Tanaka, R. Brown, N. Hondow, A. Arakaki, T. Matsunaga, S. Staniland, *J. Mater. Chem.* **2012**, *22*, 11919.
- [21] S. Staniland, W. Williams, N. Telling, G. Van Der Laan, A. Harrison, B. Ward, *Nat. Nanotechnol.* **2008**, *3*, 158.
- [22] E. Alphonse, C. Carvallo, N. Menguy, I. Chebbi, *J. Phys. Chem. C* **2011**, *115*, 11920.
- [23] J. B. Sun, F. Zhao, T. Tang, W. Jiang, J. S. Tian, Y. Li, J. L. Li, *Appl. Microbiol. Biotechnol.* **2008**, *79*, 389.
- [24] C. Lang, D. Schuler, D. Faivre, *Macromol. Biosci.* **2007**, *7*, 144.
- [25] T. Prozorov, D. A. Bazylinski, S. K. Mallapragada, R. Prozorov, *Mater. Sci. Eng., R* **2013**, *74*, 133.
- [26] J. Bain, S. S. Staniland, *Phys. Chem. Chem. Phys.* **2015**, *17*, 15508.
- [27] M. Eltayeb, E. Stride, M. Edirisinghe, *Nanotechnology* **2013**, *24*, 465604.
- [28] R. Pareta, M. Edirisinghe, *J. R. Soc. Interface* **2006**, *3*, 573.
- [29] E. Stride, M. Edirisinghe, *Soft Matter* **2008**, *4*, 2350.
- [30] B. Maherani, E. Arab-Tehrany, M. R. Mozafari, C. Gaiani, M. Linder, *Curr. Nanosci.* **2011**, *7*, 436.
- [31] W. F. Guerin, R. P. Blakemore, *Appl. Environ. Microbiol.* **1992**, *58*, 1102.
- [32] J. Gehl, *Acta Physiol. Scand.* **2003**, *177*, 437.
- [33] J. Bain, L. Ruiz-Pérez, A. J. Kennerley, S. Muench, R. Thompson, G. Battaglia, S. S. Staniland, *Nat. Sci. Rep.* **2015**, *5*, 14311.
- [34] E. Neumann, K. Tönsing, S. Kakorin, P. Budde, J. Frey, *Biophys. J.* **1998**, *74*, 98.
- [35] T. Ahn, J. H. Kim, H.-M. Yang, J. W. Lee, J.-D. Kim, *J. Phys. Chem. C* **2012**, *116*, 6069.
- [36] D. A. Bazylinski, R. B. Frankel, *Nat. Rev. Microbiol.* **2004**, *2*, 217.
- [37] M. M. Rahman, S. B. Khan, M. F. A. Jamal, A. M. Aisiri, in *Nanomaterials* (Ed: M. Rahman), InTech, Rijeka, Croatia **2011**, p. 43.
- [38] M. Samiullah, *Phys. Rev. B* **1995**, *51*, 10352.
- [39] Y. Zhang, X. Zhang, W. Jiang, Y. Li, J. Li, *Appl. Environ. Microbiol.* **2011**, *77*, 5851.
- [40] C. J. Luo, S. D. Stoyanov, E. Stride, E. Pelan, M. Edirisinghe, *Chem. Soc. Rev.* **2012**, *41*, 4708.